Microstructural and Fractographic Aspects of Corrosion Fatigue

J. I. Dickson, Li Shiqiong, and J.-P. Baïlon
Département de Génie métallurgique, École Polytechnique, P.O. 6079, Sta. "A," Montréal (Québec) Canada H3C 3A7

INTRODUCTION

The fatigue properties in aggressive environments can often be considerably lower than in inert or benign environments as a result of effects that are generally referred to as corrosion fatigue. Understanding the manner in which the microstructure influences the corrosion-fatigue behavior can be of particular importance in designing alloys and thermal or thermomechanical treatments that provide improved fatigue resistance in aggressive environments. A good understanding of the relationships between the microstructure and the corrosion-fatigue behavior can also be very useful in identifying the details of the mechanisms by which aggressive environments facilitate the initiation and propagation of fatigue cracks. Despite their importance, the corrosion fatigue–microstructure relationships have not been the subject of very many detailed studies in comparison to the number of material–environment systems in which important corrosion-fatigue effects have been identified.

The objective of the present article is, therefore, to review some of the work that has been carried out in this field in order to provide an overview of the type of effects that the microstructure can have on the fatigue crack initiation and propagation behavior in aggressive environments.

CORROSION FATIGUE CRACK INITIATION

The influence of an aggressive environment on crack initiation can include effects that facilitate the initiation of cracks, or the early stages of their propagation at crystallographic deformation features, such as slip bands and twin interfaces, and effects that cause localized corrosion of one or more microstructural constituents, such as inclusions or grain boundaries, with this localized attack giving rise to the stress or strain concentrators at which crack initiation subsequently occurs. The former type of effects can be expected to occur primarily in high-purity metals and alloys on specimens or components with polished surfaces, because it is only in the absence of significant surface defects that crack initiation occurs along crystallographic deformation features. The occurrence of fatigue-crack initiation at corrosion pits that have formed at microstructural features, such as inclusions, is common in commercial-purity materials, such as steels. Because the initiation of fatigue cracks generally occurs at the free surface, the near-surface microstructure, including the presence of surface coatings, is particularly important. It is localized corrosive attack that facilitates fatigue-crack initiation. When uniform corrosion occurs and progresses slightly more rapidly than the early progression of fa-

MATERIALS CHARACTERIZATION 28:327–347 (1992)
1044–5803/92/$5.00

tigue damage, the fatigue life tends to be prolonged.

The microstructural effects on corrosion-fatigue crack initiation will generally depend on the material composition and condition; the composition, distribution, and shape of the individual microstructural constituents; the composition of the aggressive environment; the acting electrochemical potential and electrochemical coupling effects between the phases; the surface finish; the applied stress or strain amplitudes; the temperature and the cycling frequency; and the form of the stress or strain wave. The effect of frequency, and the related effect of wave form, tend to be less critical than in the case of crack propagation, in that for crack initiation the frequency above which the corrosion fatigue effect disappears is generally much higher. In fatigue propagation, the time available for the environment to influence the crack tip region is limited by the velocity at which this region is displaced. The time available for the environment to act on fatigue initiation is only limited by the time that would be required to produce significant fatigue cracks in the absence of environmental effects.

INITIATION AT PLASTIC DEFORMATION FEATURES

Hahn and Duquette [1] found that testing Cu and Cu-8%Al single crystals under stress control in aereated 0.5N NaCl solution (with an applied anodic current of 100 $\mu A/cm^2$ for Cu) resulted in preferential dissolution causing blunting of the persistent or pronounced slip bands at which fatigue cracks initiated in air. This delayed the initiation along such bands and increased the fatigue life by a factor of approximately 3.5. Testing in the NaCl solution increased the height of slip offsets as well as the density of persistent slip bands for the Cu but not for the planar slip Cu-8%Al single crystals. The dislocation structures at the surface were also different for the Cu single crystals tested in air and in the NaCl solution. A dislocation-free zone and dipolar or vein-type dislocation structures were present in the immediate vicinity of the free surface of the specimens tested in air, but a dislocation-free zone was absent at the specimen surface for the tests in the NaCl solution. These observations were interpreted as indicating that an oxide film was required to form this zone. The dislocation structures in the near-surface region for the tests in this environment were described as a loose cellular structure, a description that fits the micrographs presented [1].

While dislocation-free zones have recently been shown to be associated with dipolar dislocation structures and favorably oriented external or internal (i.e., grain boundaries) surfaces [2] (Fig. 1), they do not appear to occur in the case of cellular structures [3] (Fig. 2). Thus, their absence at the free surface in the single crystals tested in the NaCl solution appears simply to reflect the fact that the dislocation structures observed in this region were more cellular. The more cellular dislocation structures in this surface region are typical of slip activity that is less predominantly on a single slip system. The observed increase in slip offset heights in the copper

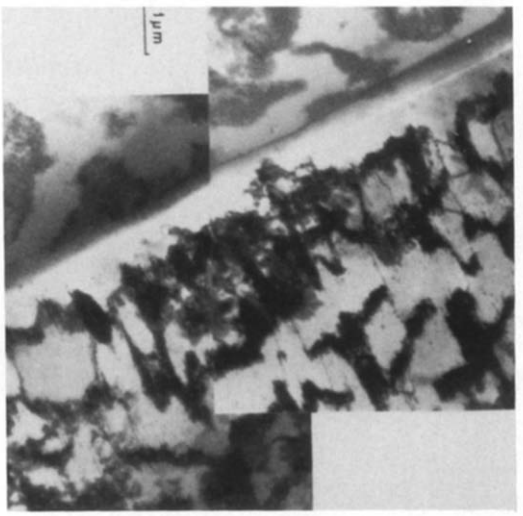

FIG. 1. Dislocation-free zone at grain boundary observed [2] for dipolar dislocation structures produced in fatigue when the dominant Burgers vector makes a large angle with the grain boundary.

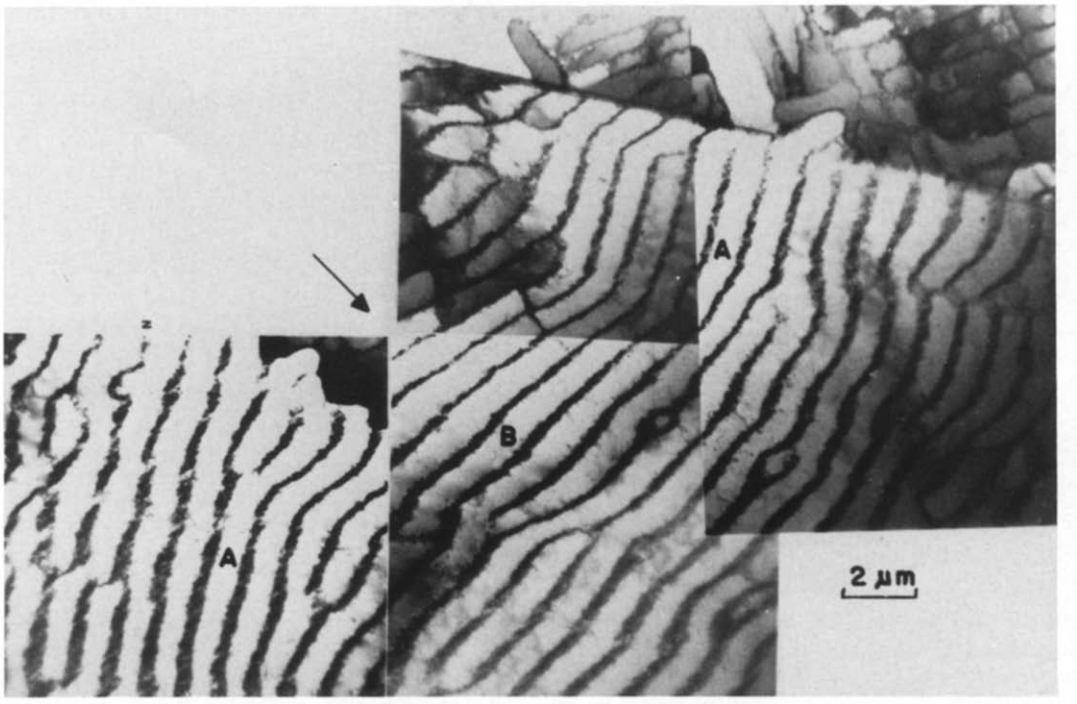

FIG. 2. Absence of dislocation-free zone at grain boundary [3] for dipolar walls (below the grain boundary) when the dominant Burgers vector is close to parallel to the grain boundary or for cellular dislocation structures (top).

single crystals was in agreement with the proposal of Duquette and Uhlig [4] and of Duquette [5, 6] that the removal of surface films permits dislocations to escape to the free surface and removes obstacles to slip, enhancing strain localization and facilitating crack initiation. It, however, is not clear how, or whether, this phenomenon gave rise to the more cellular dislocation structures and to the absence of dislocation free zones at the surfaces of the crystals tested in the NaCl solution.

Masuda and Duquette [7] had earlier observed similar persistent slip band blunting in 0.5N NaCl with applied anodic currents. For the polycrystalline material, however, the fatigue lives were reduced under applied anodic currents. This decrease was associated with a change from transgranular to intergranular crack initiation. The intergranular cracking was attributed either to preferential dissolution during cycling at dislocations accumulated at grain boundaries, or to intergranular cracking associated with strain accommodation and favored by the delayed transgranular cracking. At least part of the reduced fatigue life in the NaCl solution may be associated with the more continuous crack path for intergranular cracking than for transgranular slip band cracking, for which the microcracks encounter difficulty in crossing grain boundaries.

Collins and Duquette [8] studied the endurance and crack initiation behavior of an Al–Ni bronze tested in air and in aereated 0.5*N* NaCl solution. The microstructure consisted of rows of fcc α-grains aligned in the drawing direction with a finely dispersed eutectoid mixture of α and κ phase between α-rows and between α-grains. For tests in air, fatigue cracks initiated in the α-grain boundary regions, or along slip bands in the α-grains. The early (Stage I) crack propagation followed these slip bands, with Stage II propagation perpendicular to the applied stress following primarily the eutectoid regions. Under free

corrosion conditions in the NaCl solution, cracks initiated nearly perpendicularly to the stress axis in the eutectoid regions but initially followed slip bands after crossing into α-grains. This resulted in approximately a 30% reduction in the fatigue limit. Under applied anodic currents, one phase of the eutectoid regions was severely attacked. Cracks then initiated and propagated in these regions, and a further important reduction in fatigue life resulted. The subsequent study of Parkins and Suzuki [9] indicated that the α phase is that which is attacked in the α + κ regions. Applied cathodic currents resulted in similar crack paths as those observed in air but did not fully restore the fatigue lives to those obtained in this reference environment.

Hahn and Duquette [10] also observed slip band blunting and a transition to intergranular cracking for a solutionized IN 838 (Cu-16% Ni-0.6% Cr) alloy tested in an aereated NaCl solution. Some evidence was also found for intergranular corrosion during stress cycling under applied anodic currents, which reduced the fatigue lives with respect to those in air. The fatigue crack path in the aged alloy was mainly intergranular because of the presence of grain boundary precipitates. Testing this alloy in the NaCl solution at the free corrosion potential resulted in severe intergranular attack, a more completely intergranular cracking mode and an important decrease in the fatigue strength.

The studies of Duquette and coworkers [1, 4–10] showed the influence of prefential dissolution to retard slip band initiation when this dissolution blunted the stress concentrators produced at the slip bands. Intergranular cracking was promoted in such cases, especially when some grain boundary dissolution occurred during cycling. Moreover, the study of Hahn and Duquette [1] was the first to show the influence of an aggressive environment on the height of slip band offsets as well as on the near-surface dislocation structures.

Yan et al [11–13] studied the evolution of persistent slip bands in copper single crystals cycled under plastic strain control. One surface was immersed in deaereated 0.1*M* perchloric acid and a controlled electrochemical potential was applied to this surface. The parallel surface was in contact with a dry argon atmosphere. These test conditions of controlled strain and potential resulted in better control both of the formation of persistent slip bands and of the electrochemical reactions at the surface in contact with the aggressive environment than in the previous studies of Duquette and coworkers [1, 7]. The perchloric acid solution was chosen because it prevents the formation of surface films on copper. The effect of the aggressive environment was especially marked for the tests performed under an applied anodic potential. The maximum height of the slip offsets associated with these bands, measured by interferometry, increased by a factor of 2–3 with respect to that under open-circuit conditions. This increase in the height of the slip offsets, which resulted from having one surface in contact with the perchloric acid, continued across the bulk of the crystal and was essentially identical on the surface in contact with the argon environment. The number of persistent slip bands also increased by a similar factor. Because of the solution employed, the increase in slip line offsets under anodic polarization conditions could not be interpreted as resulting from the removal of a surface film.

In these Cu single crystals, fatigue cracks usually nucleated along the persistent slip bands that had the highest ratio of slip offset to slip band width. Testing under anodic polarization potentials resulted in a decrease in the fatigue life by approximately a factor of two with respect to that in air. Under an applied cathodic potential, the fatigue lives would have been greater than in air except that premature failure occurred in the specimen shoulders, where the crystals were protected from the environment by insulating tape. By periodically interrupting the tests carried out under an applied anodic potential, these authors [11–13] demonstrated that the per-

sistent slip bands were selectively attacked by the environment and that this localized dissolution was the predominant factor responsible for the reduction of the fatigue lives, although the strain localization phenomenon was also strongly influenced by the aggressive environment. In a test started under an applied anodic potential, slight preferential dissolution at active slip bands was shown to favor subsequent formation of persistent slip bands during the continuation of the test in air. The indication was, therefore, that the preferential dissolution and strain localization phenomena mutually enhanced each other, accounting for the synergistic interaction of the corrosion and the stress cycling on the fatigue lives. Only slight preferential dissolution occurred at persistent slip bands in the absence of simultaneous cycling and its occurrence was confined to a more limited range of anodic potentials. Yan et al [11–13] further concluded that this effect of the aggressive environment to reduce the fatigue lives occurred between two threshold values of the applied electrochemical potential. When the potential is too cathodic, the dissolution is insignificant. When the potential is too anodic, the generalized dissolution can remove the zones of fatigue damage.

Magnin and coworkers [14–18] studied the crack initiation and early stages of crack propagation during low-cycle fatigue of several stainless steels tested in air and in NaCl solutions. These steels included austenitic 316L, ferritic 26Cr–1Mo and 26 Cr–1Mo–5Ni, and austenitic-ferritic 22Cr–7Ni–2.5Mo stainless steels.

For the two former steels, they employed cellulose acetate replicas of the specimen surfaces to follow the surface propagation of small cracks [14]. The first cracks observed (surface length less than 50 μm) appeared after approximately the same number of cycles in air and in an NaCl (pH = 6) solution. The number of such microcracks, however, increased more rapidly in the NaCl solution, especially when an anodic potential was applied. The growth and coalescence of these microcracks into longer cracks was also more rapid in this solution. The anodic dissolution, resulting from the local depassivation of the steel caused at the free corrosion potential by the cyclic straining, accelerated the transition from the microcracks to the macrocracks, which eventually produced specimen fracture. In the ferritic stainless steel, the growth of the short microcracks into longer cracks occurred particularly rapidly at an applied cathodic potential (−500 mV/SCE, i.e., with respect to a saturated calomel electrode), as a result of hydrogen ions being produced in the region of the microcrack tips and giving rise to hydrogen-assisted cracking.

Magnin and Coudreuse [15, 16] also compared the low-cycle fatigue behavior of the 26Cr–1Mo and the 26Cr–1Mo–5Ni ferritic stainless steels at room temperature. For strain rates $\dot{\epsilon} > 10^{-4}\ s^{-1}$, the Fe–26Cr–1Mo steel displayed a low mobility of screw dislocations with resulting pencil glide behavior. The associated asymmetry of the deformation between tension and compression resulted in strain localization in the grain boundary regions and intergranular crack initiation. For $\dot{\epsilon} < 10^{-4}\ s^{-1}$, crack initiation remained intergranular for a solution of pH 6, but became transgranular along persistent slip bands in a solution of pH 2, as a result of the localized dissolution at these sites, following the occurrence of local depassivation. Crack initiation for $\dot{\epsilon} < 10^{-4}\ s^{-1}$ was delayed in the NaCl solution in comparison to the higher strain rates, which favored more pronounced depassivation and more difficult repassivation. For the lower amplitudes, crack initiation occurred near the grain boundaries. The 26Cr–1Mo–5Ni steel deformed by pencil glide at all strain rates tested, with important deformation twinning occurring during the first few cycles, especially at the higher amplitudes. Depending on the strain amplitudes, cracks initiated at grain boundaries, along twin interfaces or near twin-grain boundary intersections. In the NaCl solution, the occurrence of twinning, which was also ac-

companied by profuse local slip, resulted in a strong depassivation effect, as indicated by a pronounced drop in the electrochemical potential. Crack initiation then occurred very rapidly at these twins, which also acted as important microscopic stress concentrators at the specimen surface.

In the austenitic-ferritic steel [17, 18], which contained approximately 50% ferrite as bands of α-phase within an austenitic (γ) matrix, the fatigue cracks during tests in air initiated at low strain amplitudes along slip bands in the austenite. At high amplitudes, significant plastic deformation occurred in the ferrite, which showed low temperature deformation behavior with limited mobility of screw dislocations. Cracking then initiated in this phase (Fig. 3), as well as at α–α grain boundaries. At an imposed anodic potential and low amplitudes, the cracks initiated at corrosion pits in the α phase. This pitting was induced by the cyclic depassivation and occurred even below the pitting potential. At the free corrosion potential, the cracks initiated in the γ-phase at low amplitudes (Fig. 3) and in the α-phase at high amplitudes, as for the tests in air. Because the ferrite cathodically protected the austenite [17, 18], there was no reduction in fatigue life at low amplitudes. The fatigue life was reduced by half at the higher amplitudes, for which cracking initiated in the ferrite. An aging treatment at 400°C favored subsequent twinning in the ferrite and produced a considerably stronger decrease in the fatigue lives at high amplitudes, as a result of localized dissolution at the twins. Under an applied cathodic potential, the fatigue lifes were only reduced at high amplitudes for which the α-phase was deformed. This reduction in life was associated with accelerated hydrogen-assisted cracking after microcracks had formed in the α-phase.

In the type A171 and A271 duplex stainless steels with a ferritic matrix, studied by Moskowitz and Pelloux [19] and Ait Bassidi et al. [20] crack initiation in a white water environment (a solution containing chloride, sulphate and thiosulphate ions, employed in the pulp and paper industry) occurred primarily along slip bands (Fig. 4) in the softer austenitic phase. Their testing conditions favored relatively long fatigue lives in the low-cycle regime and would, therefore correspond to the lower strain amplitudes employed by Magnin et al [17, 18]. The results of Ait Bassidi et al [20] showed that the fatigue lives were de-

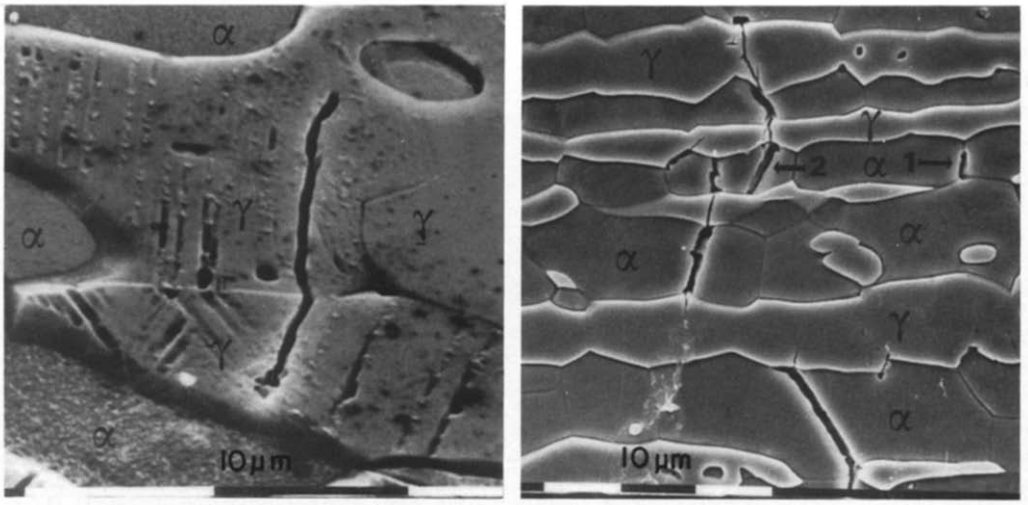

FIG. 3. (a) At low plastic strain amplitudes, Magnin et al. [17, 18] observed crack initiation in the γ phase of an austenitic-ferritic stainless steel; (b) At high amplitudes, they observed initiation at α–α grain boundaries (1) and in the α-phase (2) (courtesy T. Magnin, copyright 1987 ASTM, reprinted with permission).

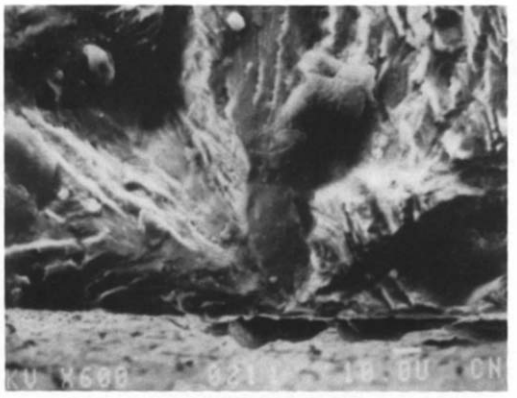

FIG. 4. Corrosion-fatigue crack initiation in KCR 171 austenitic-ferritic stainless steel has occurred at slip bands along which extrusions and, presumably, intrusions have formed [20]. Such slip bands were shown to be in the austenitic phase.

creased considerably by a decrease in the cycling frequency, which effect indicated that the stress cycling in white water facilitated crack initiation along the slip bands. For tests on these steels in air, Moskowitz and Pelloux [19] found that cracks initiated mainly along phase boundaries.

INITIATION AT CORROSION PITS

The initiation of fatigue cracks at corrosion pits has been known since early studies of corrosion fatigue [21] and has been discussed by Laird and Duquette [22] in their review article on crack initiation mechanisms during fatigue and during corrosion fatigue. These authors [22], citing the example of accelerated corrosion of Stage I cracks in low-carbon steels tested in neutral NaCl solution by Duquette and Uhlig [23], point out that care is required in order to distinguish between crack initiation, which is a consequence of corrosion pitting, and pitting, which is a consequence of previous crack initiation. A number of examples exist for which the crack initiation was clearly the result of previous pitting. A few examples will be briefly described for which corrosion pits that formed at inclusions served as the fatigue initiation sites.

Mueller [24] studied the influence of fatigue testing under stress control at 100 Hz for a 12% Cr stainless steel having a tempered martensite microstructure and an 18% Cr–2% Mo ferritic stainless steel in aerated solutions of NaCl (0.5*N* and 4*N*), adjusted to a pH of 6.5 with HCl. In the 12% Cr stainless steel, similar pitting occurred at oxide-sulfide inclusions in both solutions, and no fatigue limit was observed. The absence of such a limit is frequently reported for steels tested in aggressive environments that cause pitting. If it is assumed that a certain pit depth is required to initiate a fatigue crack that can propagate to failure at a given stress level and that this critical pit depth increases with decreasing stress, the critical pit depth can still be attained at decreasing stress levels by allowing the corrosion to proceed longer. Accordingly, a horizontal fatigue limit on a curve of stress amplitude versus log N is not obtained. The pitting behavior observed was similar in both solutions, but occurred more rapidly in the more concentrated solution, thus resulting in a lower fatigue life for a given stress amplitude.

For the 18% Cr–2% Mo stainless steel, cracking in the 4*N* solution initiated at pits produced at niobium carbonitride particles, which cracked early in the cycling, even during the tests in air. This cracking then permitted localized crevice corrosion to occur in the 4*N* solution producing the pits. While this pitting reduced the fatigue life, a fatigue limit existed, because below a certain stress amplitude corresponding to a stress level approximately 30% lower than the cyclic yield stress, the carbonitrides did not crack during cycling, and these particles no longer served as sites at which corrosion pitting initiated. This interaction between the fatigue and corrosion pitting phenomena observed in this steel is typical of the synergistic effects often obtained during corrosion fatigue, in that the stress cycling was required to cause the pitting, which, in turn, influenced the fatigue life.

In the 0.5*N* NaCl solution, the fatigue lives were intermediate between those in

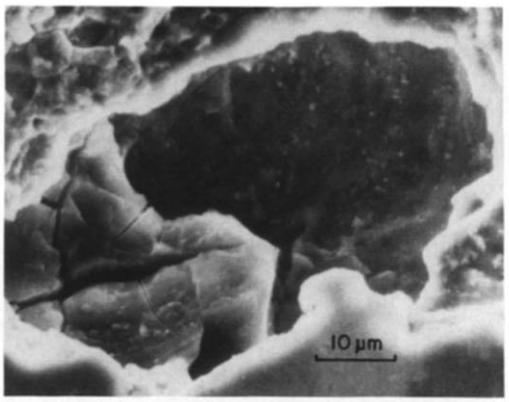

FIG. 5. Corrosion pit in martensitic CA 15 stainless steel after immersion in white water [26]. The remnants of an inclusion can be observed within the pit.

air and those in the $4N$ solution. Pitting was not observed, and the cracks initiated along slip bands. A fatigue limit again existed and was intermediate between that in air and that in the more concentrated solution. This fatigue limit was estimated as being somewhat higher than the cyclic yield stress, consistent with sufficient slip being required to rupture the passive film and to favor dissolution at the sites at which slip bands emerged on the surface.

Ait Bassidi et al. [20, 25, 26] studied the fatigue crack initiation behavior of CA-15 martensitic stainless steel tested at different cycling frequencies in a white-water environment as well as the corrosion pitting behavior of this steel in this same environment. Corrosion pits (Fig. 5) formed at the sites at which manganese sulphide inclusions intersected the surface. Such pits formed during the corrosion-fatigue tests were the usual sites of fatigue crack initiation (Fig. 6). Similar pits have also been found to be favored sites for the initiation of fatigue cracks in suction press rolls [27] made of martensitic stainless steels, which are a component of papermaking machines.

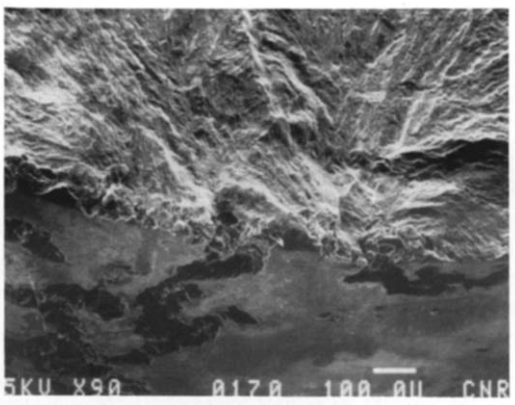

FIG. 6. Corrosion-fatigue crack initiation at a corrosion pit in CA 15 stainless steel tested in white water [26].

THE INFLUENCE OF SURFACE COATINGS

The influence of surface coatings has been discussed by Duquette [6], in his review article on crack initiation during corrosion fatigue, and will only be briefly mentioned here. Coatings that are cathodic with respect to the metal substrate are only effective as long as the coating remains unbroken and continuous. Breaks in the coating favors localized corrosion and tends to accelerate crack initiation. Coatings that are anodic with respect to the substrate can be beneficial even when there are local breaks in the coating. Electroplated zinc and cadmium coatings have been found to be beneficial in improving the corrosion-fatigue lives of steel [28]. The fatigue propagation rates of steels under cathodic protection can be accelerated for certain ranges of da/dN [29, 30]. Thus, these anodic coatings may have opposite effects on the fatigue initiation and propagation behavior. Electrochemically inert coatings are generally not effective unless they are completely continuous. It should also be remembered that some coatings can cause a significant reduction of the fatigue crack initiation life in air, which can add to the difficulty in trying to generalize their effect on the corrosion-fatigue behavior.

CORROSION FATIGUE CRACK PROPAGATION

The corrosion fatigue crack propagation process is often classified as either a stress-corrosion fatigue (SCF) or a true corrosion

fatigue (TCF) phenomenon or a combination of both [31]. Stress-corrosion fatigue is considered to include a stress corrosion contribution to fatigue cracking that acts above a threshold K_{max} value, at times assumed to be equal to K_{ISCC}, the threshold value for stress-corrosion cracking, in addition to the purely mechanical component of cracking. The true corrosion-fatigue contribution to cracking is then an environmental effect that differs from that of stress-corrosion cracking during stress cycling. The occurrence of true corrosion-fatigue phenomena also underlines the fact that corrosion-fatigue effects can occur for material-environment systems that generally do not give rise to stress-corrosion cracking effects. The classification of corrosion-fatigue propagation effects into these two broad categories is somewhat arbitrary, and tends not to take into full account the influence of the crack tip strain rates on the crack propagation behavior during both corrosion fatigue and stress corrosion cracking [32].

CRYSTALLOGRAPHY OF CRACKING

In order to identify the mechanism by which the environment accelerates corrosion fatigue, Lynch [33] carried out a series of fatigue propagation tests, generally at 1 Hz on single crystals of nickel and of Al–Zn–Mg in aggressive, inert, and liquid-metal environments.

For nickel crystals tested in a hydrogen environment, and for the Al–Zn–Mg crystals tested in distilled water and in moist air, brittle striations and accelerated crack growth were obtained. Accelerated cracking (several orders of magnitude more accelerated for the Al–Zn–Mg crystals), as well as a very similar brittle cracking mode, were obtained in the liquid-metal environments (a bismuth alloy for nickel and mercury for the Al–Zn–Mg crystals). Changes from the aggressive to the inert environment, and vice versa, resulted in very abrupt changes in the striation spacings, accompanied by a similar transition in the nature of the striations. Hydrogen precharging of specimens had no influence, during subsequent testing in inert environments, on the appearance and spacing of the striations, the aspects of which remained typical of those produced in the nonaggressive environment. Lynch [33] also performed tests at 24 Hz to determine the maximum crack velocity at which the brittle striations could be obtained in the aggressive environment. The maximum crack growth rates resulting in striations having a brittle appearance were approximately 0.02 mm/cycle for nickel and 0.2 mm/cycle for Al–Zn–Mg. These corresponded to approximate velocities of 1 and 10 mm/s, respectively, if one assumes that the crack growth in fatigue occurs during only half of the symmetrical stress cycle.

The fracture plane in the aggressive environment was crystallographic and corresponded to a {100} [33]. The crack propagation direction was <110>. At times, adjacent regions presented striations in two different <110> directions, in order to allow propagation to occur in this type of direction in each region. Considerable slip activity was observed to accompany this crack propagation mode, which produced fractographic features with a brittle appearance. The formation of the striations was reported to result from reversed slip occurring just behind the crack tip during unloading. Lynch [33] concluded that the corrosion-fatigue effect produced in these two materials was associated with the adsorption of hydrogen at the crack tip and not with the absorption of hydrogen into the material ahead of the crack tip. Only an adsorption mechanism appeared capable of accounting for the combination of a high limiting crack velocity for the occurrence of the brittle stations, of the abrupt changes in fractographic features and in interstriation spacings on changing environments and of the similarity to the fractographic features obtained for the accelerated cracking in the liquid-metal environments. The results were explained by adsorption producing localized slip in the crack tip region which, in turn, produces the environmentally enhanced cracking

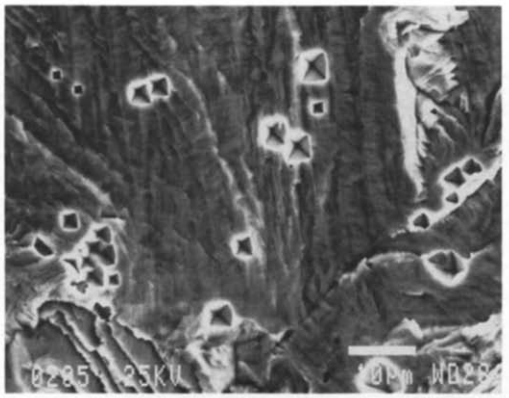

FIG. 7. Stress-corroded fracture surface for AISI 316 stainless steel tested in boiling $MgCl_2$ solution, showing {100} <110> cracking crystallography at low K [37, 38]; resulting from two sets of alternating, very fine {111} microfacets.

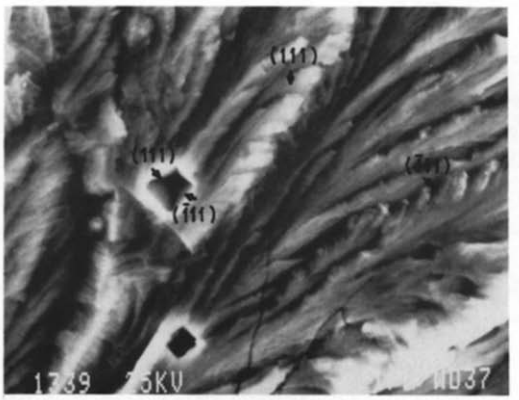

FIG. 8. More complex stress-corroded fracture surface for austenitic type 316 stainless steel at higher K, with the presence of numerous relatively large, sheetlike {111} microfacets [37, 38].

[33–35]. The resulting fracture surfaces appear brittle except when observed with sufficient resolution.

The fractography of stress-corrosion cracking (SCC) should also be closely related to that of corrosion fatigue, at least in the case of stress-corrosion fatigue (SCF). The fractographic features are generally considered identical to that of SCC, except for the presence of well-developed striations at sufficiently high ΔK, which indicate the crack arrest sites corresponding to the individual fatigue cycles.

The {100} <110> crack propagation crystallography identified by Lynch [33] in his single crystal work is the same as that identified by Dickson et al. [36], for the stress-corrosion cracking of AISI 310 stainless steel tested in boiling $MgCl_2$ solution. For type 316 stainless steel, tested in the same environment, this same crystallography (Fig. 7) was only obtained [37, 38] for low stress-intensity factors. The observations on annealed 316, as well as on cold-worked 310 stainless steels, however, demonstrated that the {100} crack plane was at least often made up of finer {111} microfacets. As K increased during the stress-corrosion cracking of 316 stainless steel, the fractographic aspects became more complex [37, 38], as a result of a tendency for the size of the {111} microfacets to increase (Fig. 8). This effect was associated with increasing crack tip plastic strains favoring larger cracking increments on the individual slip planes.

Copper and several of its alloys have been shown to crack predominantly on {110} planes during stress corrosion cracking [39–41]. The {110} facets have also been found [42] in Cu70–30Zn to consist of two sets of alternating {111} microfacets.

These observations related to the crystallography of stress-corrosion cracking, in particular, the variation of fractographic features with K for 316 stainless steel, indicate that the cracking mechanism is closely associated with the plastic deformation occurring in the crack tip region. This agrees with the conclusion of Lynch [33] that the transgranular {100} <110> cracking of brittle appearance produced during the corrosion fatigue of the fcc metals that he studied was caused by localized plastic deformation.

It is this aspect that explains the very strong similarity between the fractography of transgranular stress-corrosion cracking or corrosion fatigue and that of the transgranular fractography in the region of the fatigue threshold. Even in inert environments, the fractographic features in the region of the fatigue threshold often correspond to a {100} <110> crack propagation

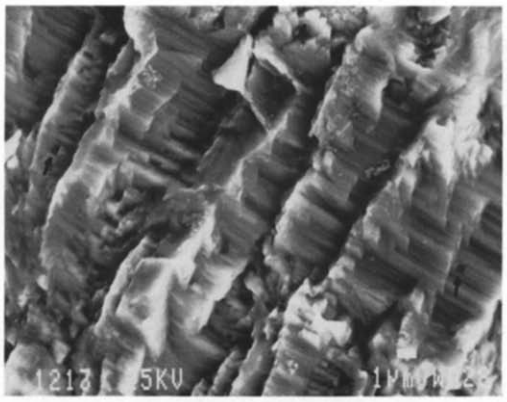

FIG. 9. Two sets of alternating {111} microfacets result in {100}<110> cracking crystallography during near-threshold fatigue in air of 70Cu–30Zn α-brass [43, 44]. The cracking crystallography can be identified from the small etch pits (arrows).

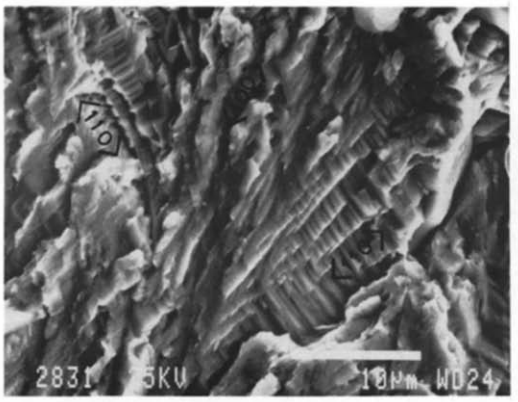

FIG. 10. Herringbone pattern produced during near-threshold fatigue of 70Cu–30Zn α-brass in air [43]. The average crack plane is {100}. Crack propagation occurs in two perpendicular <110> directions, as a result of microcracking occurring on two different sets of {111} microfacets. Between these two regions, cracking occurs in a <100> direction, and microfacets can be found corresponding to all four sets of {111} planes.

crystallography [43, 44]. In some metals, the {100} facets at times can be seen to be made up of two sets of {111} microfacets occurring in alternance. This, in particular, can be seen in metals, such as 70Cu-30Zn (Fig. 9) in which planar slip occurs, which should favor a relatively large microfacet width. Regions of {100} <100> crack propagation can also be found, in particular, between regions in which crack propagation occurs in the two different <110> directions possible for the same {100} crack plane (Fig. 10). In these intermediate regions of {100} <100> cracking, microfacets corresponding to each of the four {111} planes can, at times, be seen. In grains for which no {100} plane is well oriented, more complex fractographic features can be observed, but that are also consistent with cracking occurring on sets of {111} microfacets (Fig. 11) and that are also very similar to some of the more complicated microfractographic features produced by stress-corrosion cracking (Fig. 12). In the example seen by comparing Fig. 11 and 12, the main difference observed concerns the feathery aspect results from the tendency for stress-corrosion cracking. This feathery aspect results from the tendency for stress-corrosion cracking of annealed 316 stainless steel in the $MgCl_2$ aqueous solution to produce, at high K, fractographic features composed of sets of numerous, parallel sheetlike {111} microfacets [38].

Thus, the very strong similarity between the transgranular fractographic features of fcc metals fractured by stress-corrosion cracking and by corrosion fatigue, as well as during near-threshold (ordinary) fatigue, appears related to the crack path alternating between different microfacets

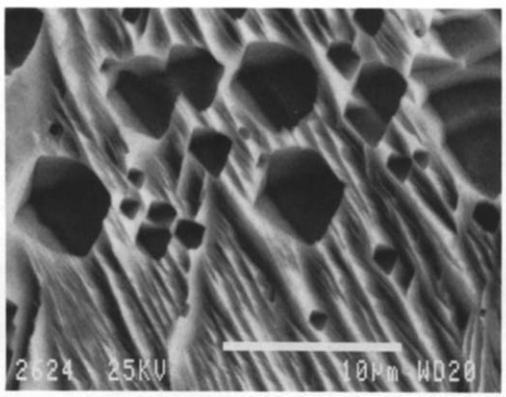

FIG. 11. Complex fractographic aspect observed [43] during near-threshold fatigue of type 316 stainless steel tested in air. The larger facets correspond to a {100}, to a near-{110} and to a {111} orientation, with the two former type of facets made up of two different sets of {111} microfacets.

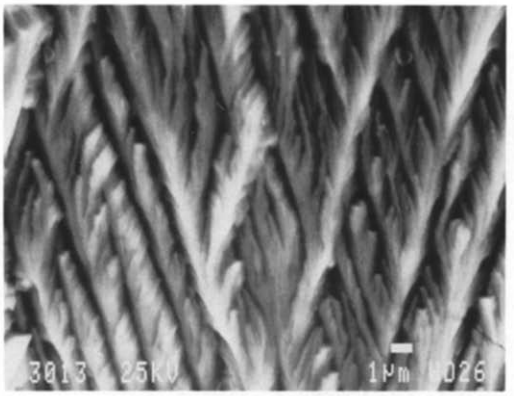

FIG. 12. Fractographic aspect of stress corrosion cracking of type 316 stainless steel tested in boiling $MgCl_2$ solution at high K [38]. The cracking crystallography can be seen to be identical to that of Fig. 11. The presence of the numerous sheetlike microfacets produced during the stress-corrosion cracking at high K is responsible for the more feathery aspect.

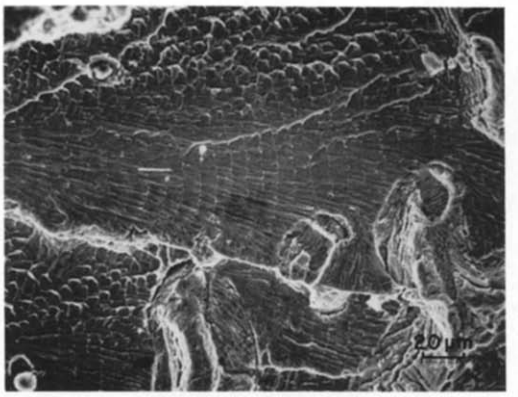

FIG. 13. Corrosion-fatigue fractographic aspect of the ferritic phase of duplex KCR 171 stainless steel tested in white water [26]. The brittle striations have a less brittle aspect near the large river lines, associated in part with a change in the inclination of the average local orientation of the fracture surface. The more ductile aspect observed here results from a greater amount of ductile stretching accompanying cracking.

that correspond to slip planes. The size of the microfacets are often so small that they are indistinguishable by scanning electron microscopy, in which case the average cracking plane corresponds well to a {100} plane, and the fractographic aspect strongly resembles that produced by cleavage.

Stubbington [45] had originally identified the {100} crack plane as that produced during corrosion-fatigue propagation of an Al-7.5% Zn-2.5% Mg alloy tested in a 3% NaCl solution. He suggested that the formation of fatigue striations included contributions from a ductile as well as from a brittle cracking process. While this suggestion does not identify the mechanism responsible for the brittle-appearing component, it does account for corrosion-fatigue facets of intermediate appearance, on which signs of significant plasticity accompanying crack propagation are clearly visible. In his studies on fcc metals, Lynch [33] had found that significant plasticity accompanied corrosion-fatigue propagation even when this was not evident from the microfractographic features.

The occurrence of such facets presenting both ductile and brittle-appearing features (Fig. 13) was studied by Ait Bassidi [25, 46, 47] on an austenitic-ferritic KCR 171 stainless steel tested in a white water environment. In these tests, it was the ferritic phase that was susceptible to corrosion-fatigue effects. The occurrence of ductile features on the brittle-appearing facets was favored by grain orientations for which the crystallographic cracking plane (also {100} in this bcc ferritic phase) was not close to perpendicular to the stress axis and for test conditions that combined high ΔK values with only a small corrosion-fatigue effect, such as in the region where the log da/dN–log ΔK curve obtained in the aggressive environment rejoined that obtained in air.

Stoltz and Pelloux [48, 49] studied the influence of the applied electrochemical potential and of the addition of sodium nitrate inhibitor on the striation morphology and on the fatigue propagation behavior of 7075-type Al alloys tested at 1 Hz in NaCl solution. Brittle striations and accelerated crack propagation with respect to tests in air were obtained in peak-aged material except when a sufficiently cathodic potential was applied (-1.4 V/SCE). Polarity reversal of the applied potential, for ΔK values of approximately 10 $MPa(m)^{1/2}$, resulted [48] in a change in orientation of the local fracture plane from a crystallographic

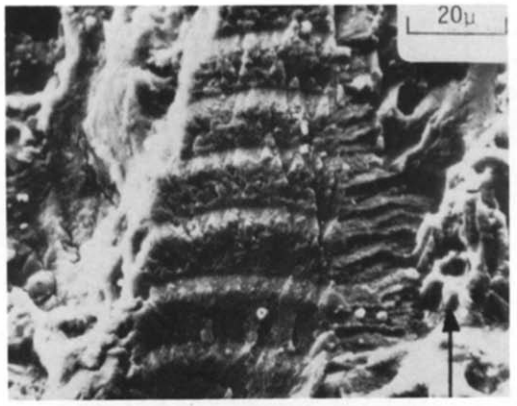

FIG. 14. Changes in the fractographic aspects of peak-aged 7075 Al alloy tested in 3.5% NaCl solution, associated with reversals of the polarity of the applied electrochemical potential [48]. The cracking in well-oriented grains is crystallographic, except when the applied potential becomes sufficiently cathodic (courtesy of R. M. Pelloux, copyright 1972, *Metallurgical Transactions*, reprinted with permission).

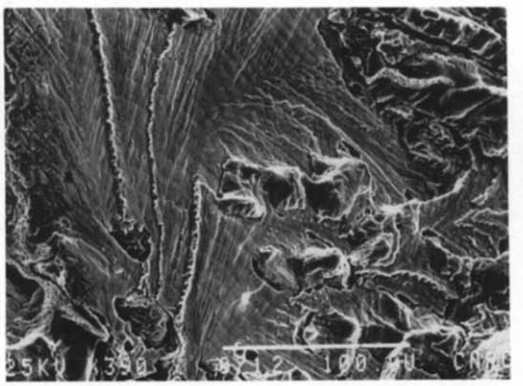

FIG. 15. Fractographic aspect of corrosion fatigue of KCR 171 duplex stainless steel, tested in white water [26, 46, 47]. Widely spaced brittle striations are observed in the ferritic matrix, and finely spaced ductile striations in the austenite. The crack front in the ferrite bypasses the austenitic grains, which then fracture in much the same manner as low-cycle fatigue specimens.

plane to a plane perpendicular to the tensile stress axis (Fig. 14). The threshold cathodic potential required not to obtain the crystallographic facets was also evaluated as approximately -1.4 V (SCE). At higher ΔK, only the aspect of the striations changed on polarity reversal, which effect was attributed to the crack tip plastic zone size becoming larger than the grain size. The addition of a sufficient concentration of sodium nitrate to the NaCl solution also resulted in an abrupt change from brittle to ductile striations and in a return to fatigue crack growth rates similar to those obtained in air. The influence of this inhibitor on the fatigue behavior was interpreted as indicating a corrosion-fatigue mechanism associated with an adsorption phenomenon or with a surface film.

CORROSION-FATIGUE IN MULTIPHASE ALLOYS

The fractographic aspects observed on the individual phases in dual-phase or multiphase alloys can be particularly useful in determining the influence of microstructure on the corrosion-fatigue behavior. Examples will be considered for austenitic-ferritic and martensitic-ferritic stainless steels, as well as for a ferritic-pearlitic structural steel and for Mn-Ni-Al bronzes.

In austenitic-ferritic KCR 171 tested in a whitewater environment by Ait Bassidi et al. [46, 47], brittle striations were present in the ferritic phase, while the striations remained ductile in the austenitic phase (Fig. 15). The interstriation spacings in the ferritic phase could be as much as 10 times larger than in the austenitic phase. The difference in the crack growth rates between the two phases could result in the grains of austenite within the ferritic matrix being bypassed by the local crack front in the ferrite (Fig. 15). These islands of austenite then fractured behind the crack front in the ferrite. The initiation of cracking in the individual austenite grains occurred at several sites around their perimeter in the plane corresponding to the crack in the ferrite. Final fracture of the center of each austenite grain generally occurred by necking or crack tip stretching of the ligament remaining between the individual cracks that had initiated in the grain. Thus, these islands of austenite fractured in a manner resembling low-cycle fatigue specimens. Once the crack front bypasses γ-grains, the cyclic strain amplitudes acting on the bypassed grains increases, accelerating the

rate at which they fracture. There was no evidence, however, to suggest that the austenitic phase was itself subject to corrosion-fatigue effects in this environment. The macroscopic crack growth rates were also found to agree quite well [26] with those indicated from the interstriation spacing in the ferritic phase. Because of the continuous nature of this more brittle phase, this result is to be expected. It, however, should not be interpreted as indicating that the presence of the austenitic phase has little influence in limiting the overall or macroscopic crack growth rate. The presence of the uncracked islands of austenite behind the crack front in the ferrite tends to limit the cyclic crack opening displacement values, ΔCTOD, which are obtained at the crack tip in the ferrite. The interstriation spacing in the ferrite also was observed [46, 47] to decrease in passing between two closely-spaced austenite grains, also in keeping with the effect of these yet uncracked grains to limit the ΔCTOD acting on the local crack front in the ferrite.

Some similar observations have also been made by Moskowitz and Pelloux [19] on the austenitic-ferritic stainless steels that they tested in a whitewater environment. These authors employed the term *keying effect* to describe the influence of the uncracked islands of austenite to limit the environmentally accelerated crack growth rates obtained in the ferrite.

Several fractographic features [46, 47] suggested a hydrogen embrittlement mechanism, including the absence of brittle striations in the plane stress regions near the lateral edges (Fig. 16) and the presence of similar brittle features for tests in air (35–45% relative humidity) in well-oriented (a {100} fracture plane almost perpendicular to the stress axis) ferrite grains. A few sites were found where reinitiation in a ferrite grain at an α–γ interface had occurred apparently ahead of the macroscopic crack front (Fig. 17); however, because of the usual presence of some decohesion at this interface, the possibility of contact with the white water at the moment of reinitiation could generally not be

FIG. 16. Absence of brittle striations near the lateral edges of KCR 171 specimens tested at 1 Hertz in white water [26, 46, 47].

ruled out. The same type of brittle striations, moreover, were subsequently observed by Kaczorowski et al [50] in Fe–3% Si single crystals fatigue tested in gaseous hydrogen.

For tests performed on CA-15 (a martensitic stainless steel containing less than 10% δ-ferrite) in the same white-water environment [26], the same type of brittle striations and accelerated cracking were again obtained in the ferrite (Fig. 18), with

FIG. 17. Initiation, at α–γ interface, of cleavage-like corrosion-fatigue cracking in a ferritic grain of KCR 171 ahead of the macroscopic crack front. The ductile striations in the austenitic grain on the other side of this interface indicate local cracking propagating back toward the macroscopic crack front.

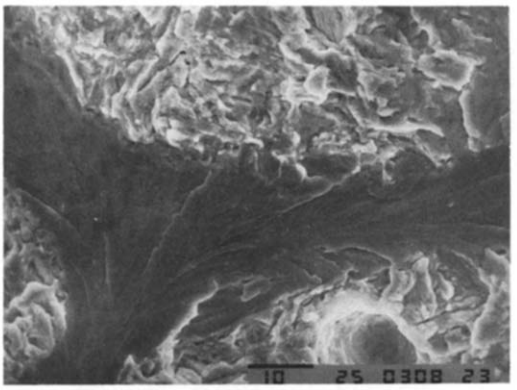

FIG. 18. Fractographic aspect of corrosion fatigue of CA 15, a martensitic stainless steel containing approximately 10% of δ-ferrite, tested in white water [26]. Accelerated cracking is obtained in the ferrite, accompanied by cleavagelike facets and brittle striations; finely spaced ductile striations are obtained in the martensite. The cracking in the ferrite proceeds ahead of the macroscopic crack front and facilitates, at the interphase boundaries, the initiation of cracking in the martensite.

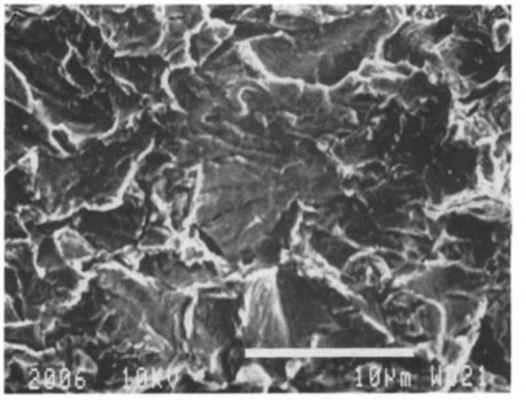

FIG. 19. Fractographic aspect of corrosion fatigue of a structural steel for offshore applications tested in synthetic sea water, under an applied cathodic potential (−1000 mV/SCE) [30]. Highly crystallographic brittle striations are obtained in the ferrite; ductile striations are obtained in the pearlite present near the ferritic grain boundaries.

finer, more ductile striations present in the martensite. The crack propagation in the martensite bordering the ferritic grains proceeded laterally from the interface with these grains. Most of the acceleration of the macroscopic growth rates appeared to be related to the hydrogen-assisted cracking in the ferrite proceeding ahead of the macroscopic crack front and initiating lateral cracking in the surrounding martensite.

The same type of brittle fractographic features were also observed on corrosion-fatigue fracture surfaces [30] of an offshore ferritic-pearlitic steel for tests under cathodic protection (−1.0 V/SCE). Again in this steel, these cleavage like facets with brittle striations were only present in the ferrite (Fig. 19). Ductile striations were present in the pearlite.

These different observations demonstrate how ferrite can be susceptible to hydrogen-enhanced fatigue crack propagation even in cases when harder microstructural constituents (such as martensite and pearlite) in the same steels are not, or are little, affected. It would, however, appear premature to try to extrapolate this type of behavior to other steels, for which this aspect has not been verified.

Dickson et al [51–53] studied the corrosion-fatigue propagation of 12%–14% Mn-8% Al-2% Ni-3% Fe ship propeller bronzes at the free corrosion potential in a 3.5% NaCl solution. Several material conditions were tested. The laboratory as-cast (AC) condition (25.4-mm-thick plates) simulated the microstructure of keel blocks. A subsequent 2-h anneal at 900°C followed by cooling at 10°C/h to 230°C resulted in slowly-cooled (SC) material having a microstructure that simulated, reasonably well, that of large castings. The third material condition studied, denoting the HT condition, was obtained by annealing the SC material for 2h at 690°C, followed by water quenching.

These bronzes contained two principal phases, with the fcc α-phase present as smaller grains within larger bcc β-grains. κ particles rich in iron and manganese were also present, generally within α-grains. For the AC and SC conditions, the β-ligaments between α-grains were narrow (Fig. 20). The annealed and quenched (HT condition) resulted in a higher-volume fraction of β-phase and a considerably

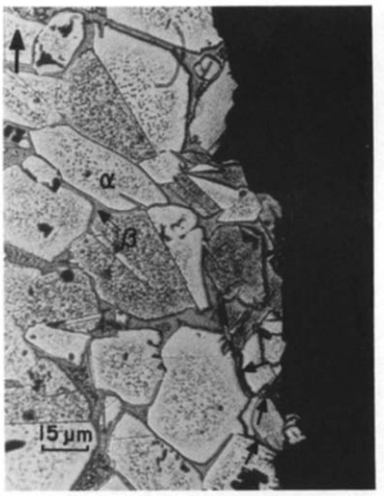

FIG. 20. Metallographic section at a corrosion-fatigue surface of a 12% Mn-8% Al-2% Ni bronze in the SC condition [53]. Some decohesion can be seen at α–β interfaces within 30 μm of the fracture surface.

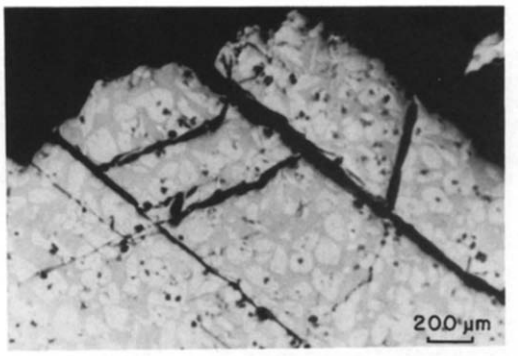

FIG. 22. Secondary crack observed next to the fracture surface on a metallographic section of a 12% Mn-8% Al-2% Ni bronze, fatigue tested in 3.5% NaCl solution [51, 52]. The relatively straight crack path in both phases indicates that the crack encounters little difficulty in crossing α–β grain boundaries.

thicker amount of β-phase surrounding the α-grains (Fig. 21 and 22).

The general behavior observed was that of accelerated corrosion-fatigue crack propagation at the higher ΔK values in the aggressive environment, with the difference between the crack growth curves in the NaCl solution and in air increasing with increasing ΔK up to the highest da/dN values employed in the tests (10^{-3} to 2×10^{-3} mm/cycles). Below approximately 10^{-5} mm/cycle, testing in the NaCl solution resulted in considerable corrosion-product induced crack closure effects and in slower crack growth rates than those obtained in air for similar nominal ΔK values.

The microfractographic evidence [51–53] indicated that the accelerated corrosion-fatigue propagation for the AC and SC conditions was essentially the result of decohesion (Fig. 23) being produced during

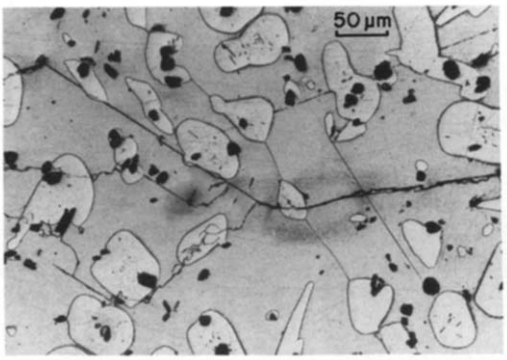

FIG. 21. Secondary crack observed near the fracture surface on a metallographic section of a 12% Mn-8% Al-2% Ni bronze, fatigue tested in air [51, 52]. The tortuous crack path in both phases, but particularly in the α-phase, indicates that crossing into α-grains is difficult.

FIG. 23. The corrosion-fatigue fracture surface of the 12% Mn-8% Al-2% Ni bronze in the SC condition [51–53]. Decohesion at the α–β interfaces has proceeded ahead of the macroscopic crack front and facilitated the initiation of fatigue cracking in the adjacent α-grains. The large arrow indicates the macroscopic crack propagation direction; the small arrows indicate local crack propagation directions.

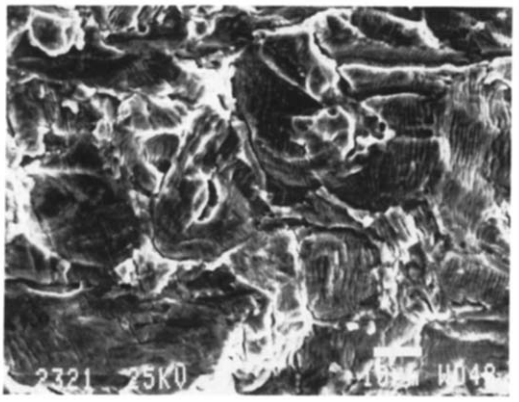

FIG. 24. Fractograph of the 12% Mn-8% Al-2% Ni bronze in the SC condition fatigue tested in air [53]. The aspect of the striations indicates that the crack propagated in a straightforward manner from grain to grain. There is no indication of decohesion at α–β interfaces proceeding ahead of the macroscopic crack front.

tests in the NaCl solution along the portions of the α–β interfaces that intersected the macroscopic crack front. Such features were not present on the fracture surfaces produced in air (Fig. 24). These interface cracks proceeded ahead of the macroscopic crack front and facilitated crack initiation at different sites in the adjoining α-grains and possibly in the adjoining β-ligaments, although the latter could not be determined fractographically, because of the very limited plasticity in the β-phase. The fatigue striations in the α-grains (Fig. 23) permitted to follow the local crack path and to identify the approximate crack initiation sites within each grain. Ridge lines separating the portions of cracks that initiated on different parallel planes also permitted to identify the initiation sites within the individual α-grains. The decohesion at the α–β interface could also be observed in the immediate vicinity of the fracture surface on metallographic profile sections (Fig. 20).

This crack path somewhat resembles that observed by Parkins and Suzuki [9] for the stress-corrosion cracking of a Ni-Al bronze tested in natural sea water. For the lower applied potentials, cracking occurred at the α-κ interfaces. Their observations also indicated some preferential dissolution of the α-phase at the more anodic potentials. They also found that cycling in sea water reduced the threshold stress level for fatigue cracking of smooth specimens. They interpreted the environmentally enhanced cracking of this Ni-Al bronze as resulting essentially from a dissolution mechanism. A dissolution mechanism, however, appears inconsistent with the results on the Mn-Ni-Al bronzes, for which the maximum corrosion fatigue effect obtained occurred at the highest growth rates attained during the tests. Dickson et al [51–53] attributed the environmentally produced decohesion at the α–β interfaces to a stress-sorption effect. Mshana et al [54] obtained the log da/dN–log ΔK curves for 8.5%–9.5% Al–4%–5% Ni alloy in 3% NaCl and in air and did not observe any clear corrosion-fatigue accelerated crack propagation. It appears, therefore, that the environmentally assisted cracking mechanism differs in the Mn–Al–Ni bronzes from that in the Al–Ni bronzes.

For the Mn–Al–Ni bronzes in the HT condition [52, 53], the fatigue crack in the β-phase during tests in air tended to bypass the α-grains at the higher da/dN values. Fatigue cracking within the bypassed α-grains occurred subsequently from two or more initiation sites along the perimeter of these grains. This could be observed either from the fracture surface (Fig. 25) or from the secondary cracks on metallographic sections intersecting the fracture surface (Fig. 21). The crack path within α-grains was often tortuous. For the tests in the NaCl solution, the crack front passed with little difficulty from the β- to the α-phase. This can be seen fractographically (Fig. 26) or metallographically (Fig. 22), from the tendency of the secondary cracks to be straighter within β-grains and not tortuous within the α-grains.

Thus, while the microscopic details of the corrosion-fatigue crack path for the Mn–Al–Ni bronze differed for the HT condition compared to that for the AC or SC conditions, in all cases, the accelerated cracking in the NaCl solution involved the

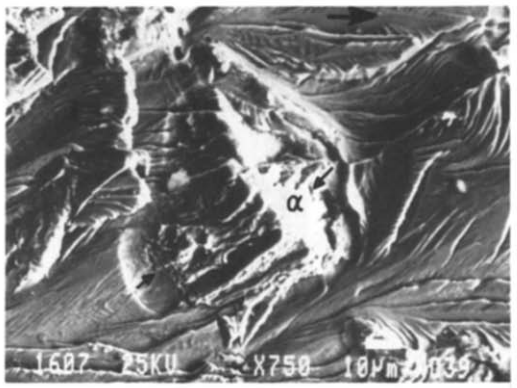

FIG. 25. Fractograph of the 14% Mn-8% Al-2% Ni bronze in the HT condition fatigue tested in air [51, 52]. Cracking in the β-phase bypassed the α-grain, which later fractured behind the crack front in the β-phase. The two small arrows indicate the local crack propagation direction near the two fatigue initiation sites in the α-grain.

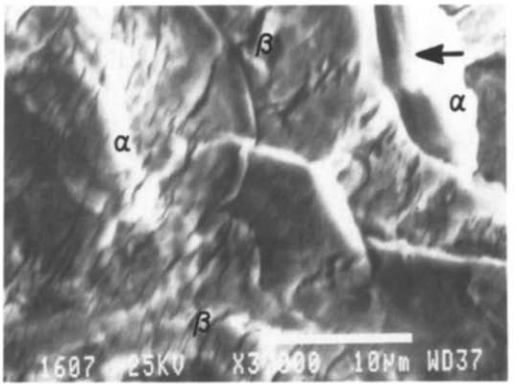

FIG. 26. Fractograph of the 14% Mn-8% Al-2% Ni bronze in the HT condition fatigue tested in 3.5% NaCl solution [51, 52]. The ductile striations indicate that the crack encountered little difficulty in crossing α–β grain boundaries.

passage of cracking into α-grains being facilitated by the aggressive environment.

INFLUENCE OF INCLUSIONS ON HYDROGEN-ASSISTED FATIGUE CRACKING

That inclusions and other second-phase particles can have an influence on hydrogen-assisted crack propagation under monotonic loading is well known. Hydrogen absorbed in the material ahead of the crack tip can cause local crack initiation in the region of the inclusions in the crack tip plastic zone ahead of the macroscopic crack front [55] and cause the crack propagation plane to deviate and follow a path containing a high density of inclusions or second-phase particles that are sites at which hydrogen trapping tends to occur. Similar behavior can also be observed in hydrogen-enhanced fatigue crack propagation. In structural steels, it is known that the accelerated cracking obtained in aqueous environments can depend on the sulphur content of the steel [55]. Torronen et al [57] observed that this dependence on the sulphur content was more precisely a dependence on the number, size, shape and distribution of the sulphide inclusions.

In the study by Torronen et al [57] of the fatigue of two pressure vessel steels in pressurized, high-temperature (288°C), low-oxygen (<100 ppb), high-purity water, brittle-appearing fractographic features accompanied the occurrence of accelerated cracking in ASTM A 533 B C1 steel. These brittle-appearing fractographic facets fanned out from regions of high densities of elongated manganese sulphide inclusions. Regions with ductile striations, and lower densities of these inclusions, were present between the zone of brittle fractographic features, although a few brittle facets were also associated with some inclusions within the regions having a more ductile appearance. The crack growth rates at a given ΔK value were considerably lower, and the zones of brittle fractographic features were not observed for the second steel that they studied, a Cr–Mo–V steel, for which the inclusions were round, smaller, and more evenly distributed.

These authors [57] further suggested that the inclusions were related to the threshold stress intensity factor above which hydrogen-assisted fatigue cracking occurred, through the stress concentration associated with the inclusions present in the crack tip plastic zone. The stress concentration would be considerable lower for

small round inclusions than for elongated inclusions.

The observations of Torronen et al [57] indicated that brittle-appearing fracture zones initiated ahead of the macroscopic crack front and were associated with the trapping of hydrogen in the regions of the manganese sulphide inclusions. They also pointed out that the dissolution of these sulphide inclusions in the crack tip region can contribute to this cracking by influencing the the local electrochemical conditions. Sulfides in aqueous solution are known to act as a poison for the formation of H_2 gas molecules and thus favor hydrogen absorption into the steel, further contributing to the hydrogen-enhanced cracking.

CONCLUSIONS

Corrosion-fatigue behavior can be associated with different phenomena that give rise to accelerated crack initiation and/or crack propagation. Comparison with similar fractographic features obtained during stress-corrosion cracking and during near-threshold fatigue indicates that the brittle-appearing fractographic facets produced by corrosion fatigue in fcc metals result from the crack path alternating between different {111} slip planes.

The microstructure often has a strong influence on the corrosion-fatigue behavior, and knowledge of this influence is necessary in order to properly understand this behavior. Knowledge of the influence of the microstructure consequently can be particularly useful in improving the resistance to corrosion-fatigue through microstructural modifications.

Financial support from the FCAR (Quebec) and NSERC (Canada) research-support programs is gratefully acknowledged. The authors are grateful to Profs. Thierry Magnin and Regis Pelloux for permission to republish Fig. 2 and 14 which appeared in references [17] and [48], respectively. The authors are also grateful to ASTM and Metallurgical Transactions, for permission to republish these micrographs. The authors express their gratitude to Mustapha Ait Bassidi for permission to publish several of the previously unpublished micrographs from his Ph.D. thesis.

References

1. H. N. Hahn and D. J. Duquette, The effect of surface dissolution on fatigue deformation and crack nucleation in copper and copper-8% aluminum single crystals, *Acta Metall.* 26:279 (1978).
2. J. I. Dickson, Hong Bande, S. Turenne and G. L'Espérance, The occurrence of dislocation-free zones at grain boundaries and free surfaces during cyclic deformation, *Mater. Sci. Eng.* 89:L31 (1987).
3. J. Boutin, Fatigue oligocyclique du cuivre et du laiton 70/30: comportement cyclique, influence de la taille de grains et contraintes internes et effectives, M. App. Sc. Thesis, Ecole Polytechnique de Montréal (1983).
4. D. J. Duquette and H. H. Uhlig, The critical reaction rate for corrosion fatigue of 0.18% carbon steel and the effect of pH, *Trans. ASM* 62:839 (1969).
5. D. J. Duquette, A review of aqueous corrosion fatigue, *Corrosion Fatigue: Chemistry, Mechanics and Microstructure* (O. F. Deverux, A. J. McEvily and R. W. Staehle, eds.), NACE, Houston, (1972), p. 12.
6. D. J. Duquette, Environmental effects I: general fatigue resistance and crack nucleation in metals and alloys, *Fatigue and Microstructure*, ASM, Metals Park, (1979), p. 335.
7. H. Masuda and D. J. Duquette, The effect of surface dissolution on fatigue crack nucleation in polycrystalline copper, *Met. Trans. A*, 6A:87 (1975).
8. P. Collins and D. J. Duquette, Corrosion fatigue behavior of a duplex aluminum bronze alloy, *Corrosion (NACE)* 34:119 (1978).
9. R. N. Parkins and Y. Suzuki, Environment sensitive cracking of a nickel-aluminium bronze under monotonic and cyclic loading conditions, *Corros. Sci.* 23:577 (1983).
10. H. N. Hahn and D. J. Duquette, The effect of heat treatment on the fatigue and corrosion fatigue behavior of a CuNiCr alloy, *Met. Trans. A* 10A:1453 (1979).
11. B. D. Yan, G. C. Farrington, and C. Laird, Strain localization enhanced by preferential dissolution in corrosion fatigue—a threshold effect, *Fatigue 84*, (C. J. Beevers, ed.), EMAS Ltd., Warley, Vol. III, (1984) p. 1435.
12. B. D. Yan, G. C. Farrington, and C. Laird, Strain localization in single crystals of copper cycled in

0.1 M perchloric acid solution under potential control, *Acta Metall.* 33:1533 (1985).

13. B. D. Yan, G. C. Farrington, and C. Laird, The interaction of simultaneous cyclic straining and aqueous corrosive attack in the behavior of persistent slip bands, *Acta Metall.* 33:1593 (1985).
14. T. Magnin and C. Ramade, Evolution of microcracks during low cycle fatigue in aqueous corrosive solutoins, *Low Cycle Fatigue and Elasto-Plastic Behavior of Materials*, (K. T. Rie, ed.), Elsevier Applied Science, London (1987), p.354.
15. T. Magnin and L. Coudreuse, The influence of plastic deformation mechanisms on the corrosion-fatigue behaviour of ferritic stainless steels, *Fatigue 84* (C. J. Beevers, ed.), EMAS Ltd, Warley, Vol. III, (1984), p. 1447.
16. T. Magnin and L. Coudreuse, Corrosion fatigue mechanisms in B. C. C. stainless steels, *Acta Metall.* 35:2105 (1987).
17. T. Magnin, J. M. Lardon, and L. Coudreuse, A new approach to low cycle fatigue behavior of a duplex stainless steel based on the deformation mechanism of the individual phases, *Low Cycle Fatigue.* (H. D. Solomon, G. R. Halford, L. R. Kaisand, and B. N. Leis eds.) ASTM STP 942, ASTM, Philadelphia, (1987), p. 812.
18. T. Magnin, J. M. Lardon, and C. Amzallag, Coupling effects between the alpha and gamma phases during corrosion fatigue of an alpha-gamma duplex stainless steel, *Fatigue 87* (R. O. Ritchie and E. A. Starke Jr., eds.), EMAS Ltd, Warley, Vol. III, (1987), p. 1221.
19. J. A. Moskowitz and R. M. Pelloux, Corrosion-fatigue behavior of austenitic-ferritic stainless steels, *Corrosion Fatigue Technology*, ASTM STP 642 (H. L. Craig, Jr., T. W. Crooker, and D. W. Hoeppner, eds.), ASTM, Philadelphia, (1978), p. 133.
20. M. Ait Bassidi, J. Masounave, and J. I. Dickson, The corrosion-fatigue behavior in White Water of KCR 171, *Duplex Stainless Steels* (R. A. Lula, ed.), ASM, Metals Park, OH, (1983), p. 445.
21. D. J. McAdam, Jr., and G. W. Geil, Pitting and its effect on the fatigue limit of steels corroded under various conditions, *Proc. ASTM* 41:696 (1941).
22. C. Laird and D. J. Duquette, Mechanisms of fatigue crack nucleation, *Corrosion Fatigue: Chemistry, Mechanics and Microstructure* (O. F. Devereux, A. J. McEvily, and R. W. Staehle, eds.), NACE, Houston, (1972), p. 88.
23. D. J. Duquette and H. H. Uhlig, Effect of dissolved oxygen and NaCl on corrosion fatigue of 0.18% carbon steel, *Trans. ASM* 61:449 (1968).
24. M. P. Mueller, Dependence of corrosion fatigue crack initiation mechanisms on the corrosion behavior of two stainless chromium steels, *Corrosion (NACE)* 8:431 (1982).
25. M. Ait Bassidi, J. Masounave, and J. I. Dickson, A study of the effect of white water on fatigue in some stainless steels, *Pulp and Paper Industry Corrosion Problems*, Vol. 4: (1983), p. 108, Swedish Corrosion Institute, Stockholm.
26. M. Ait Bassidi, Etude des mécanismes de fissuration par fatigue corrosion de différents types d'aciers inoxydables, Ph. D. Thesis, École Polytechnique de Montréal (1983).
27. A. Garner, Suction roll failures in Canada, *Pulp and Paper Canada* 86:T62 (1985).
28. N. Stuart and U. R. Evans, The effect of zinc on the corrosion-fatigue life of steel, *J. Iron and Steel Inst.* 147:131 (1943).
29. T. W. Thorpe, P. M. Scott, A. Rance, and D. Silvester, Corrosion fatigue of BS 4360:50D structural steel in seawater, *Intern. J. Fatigue* 5:123 (1983).
30. J. I. Dickson, Y. Blanchette, and J. -P. Bailon, The effect of cathodic protection on the propagation of long and short fatigue cracks, *Cathodic Protection: a + or − in Corrosion Fatigue* (O. Vosikovsky and K. Leewis, eds.), CANMET, Ottawa, (1986), p. 57.
31. A. J. McEvily and R. P. Wei, Fracture mechanics and corrosion fatigue, *Corrosion Fatigue: Chemistry, Mechanics and Microstructure* (O. F. Devereux, A. J. McEvily, and R. W. Staehle, eds.), NACE, Houston, (1972), p. 88.
32. R. N. Parkins and B. S. Greenwell, The interface between corrosion fatigue and stress corrosion cracking, *Metal Sci.* 11:405 (1977).
33. S. P. Lynch, Mechanisms of environmentally assisted fatigue in nickel and Al-Sn-Mg single crystals, *Fatigue 84*, Vol. (C. J. Beevers, ed), EMAS Ltd., Warley, I: (1984), p. 445.
34. S. P. Lynch, Cleavage fracture in face-centred cubic metals, *Metal Science* 15:463 (1981).
35. S. P. Lynch, Environmentally assisted cracking: overview of evidence for an adsorption-induced localized slip process, *Acta Metall.*, 36:2639 (1988).
36. J. I. Dickson, D. Groulx, Li Shiqiong, and D. Tromans, The fractography of SCC of 310 stainless steel: crystallographic aspects and influence of K, *Mater. Sci. Eng.* 94:155 (1987).
37. J. I. Dickson, Li Shiqiong, J. -P. Bailon, and D. Tromans, Fractographic and crystallographic aspects of stress corrosion cracking in 316 stainless steel, *Microstructural Sci.* 15:251 (1987).
38. Li Shiqiong, J. I. Dickson, J. -P. Bailon, and D. Tromans, The influence of stress intensity factor on the fractography of stress corrosion cracking of 316 stainless steel, *Mater. Sci. Eng.*, A119:59 (1989).

39. E. I. Meletis and R. F. Hochmann, Techniques for determination of the crystallographic characteristics of environmentally induced brittle fractures, *J. Testing Eval.* 12:142 (1984).
40. J. L. Nelson and J. A. Beavers, The propagation of transgranular stress corrosion cracks in admiralty metal, *Metall. Trans. A* 11:809 (1980).
41. R. Bakish, Cleavage steps and the cleavage plane in chemically embrittled Cu_3Au Single crystals, *Trans. AIME* 209:494 (1957).
42. J. I. Dickson, Li Shiqiong, and J.-P. Bailon, Aspects fractographiques de la corrosion sous contrainte, *Corrosion sous Contrainte*, Editions de Physique, Paris (to be published in 1992).
43. J. I. Dickson, Li Shiqiong, and J. -P. Bailon, An explanation of the fractography of near-threshold fatigue in F. C. C. metals, *Fatigue 87*, Vol. II (R. O. Ritchie and E. A. Starke, J., eds), EMAS Ltd., Warley; (1987), p. 759.
44. J. P. Bailon, J. I. Dickson, and Li Shiqiong, Relationship betwen fractographic features and fatigue propagation mechanisms at or near the threshold, *Basic Mechanisms in Fatigue of Metals* (P. Lukas and J. Polak, eds.) Academia, Prague, (1988), p. 361.
45. C. A. Stubbington, Some observations on air and corrosion-fatigue of an aluminium-7.5% zinc-2.5% magnesium alloy, *Metallurgia* 68:109 (1963).
46. M. Ait Bassidi, J. Masounave, J. -P. Bailon, and J. I. Dickson, Fractographic study of corrosion-fatigue crack propagation in a duplex stainless steel, *Defects, Fracture and Fatigue* (G. W. Sih and J. W. Provan, eds.), Martinus Nijhoff, The Hague, (1983), p. 359.
47. M. Ait Bassidi, J. Masounave, J. I. Dickson, and J.-P. Bailon, Fatigue-corrosion de l'acier austéno-ferritique KCR 171 dans l'eau blanche, *Can. Metall. Quart.* 23:17 (1984).
48. R. E. Stoltz and R. M. Pelloux, Mechanisms of corrosion fatigue crack propagation in Al-Sn-Mg alloys, *Met. Trans.* 3:2433 (1972).
49. R. E. Stoltz and R. N. Pelloux, Inhibition of corrosion fatigue in 7075 aluminum alloys, *Corrosion (NACE)* 29:13 (1973).
50. M. Kaczorowski, C. -S. Lee, and W. W. Gerberich, Dislocation distributions associated with fatigue cracking on cleavage planes, *Mater. Sci. Eng.* 81:305 (1986).
51. J. I. Dickson, L. Handfield, S. Lalonde, M. Sahoo, and J.-P. Bailon, Corrosion-fatigue crack propagation behaviour of Mn-Ni-Al bronze propeller alloys, *J. Mater. Eng.* 10:45 (1988).
52. J. I. Dickson, L. Handfield, S. Lalonde, M. Sahoo, and J.-P. Bailon, The corrosion-fatigue crack propagation behavior of Mn-Ni-Al Bronze, *Corrosion Cracking* (V. S. Goel, ed.) ASM, Metals Park, OH (1986), p. 279.
53. J. I. Dickson, L. Handfield, J. -P. Baïlon, and M. Sahoo, The fatigue and corrosion-fatigue crack growth behaviour of a Mn-Ni-Al bronze, *Fatigue 84*, Vol. I, (C. J. Beevers, ed.), EMAS Ltd., Warley, (1984), p. 191.
54. J. S. Mshana, O. Vosikovsky, and M. Sahoo, Corrosion fatigue behaviour of Ni-Al bronze alloy, *Can. Metall. Quart.* 23:7 (1984).
55. J. I. Dickson and J. P. Bailon, The fractography of environmentally-assisted cracking, *Time-Dependent Fracture* (A. S. Krausz, ed.), Martinus Nijhoff, Dordrecht, (1985), p. 69.
56. C. Amzallag and J. L. Bernard, *Proceedings of IAEA Specialists Meeting on Subcritical Crack Growth*, Freiburg, (1981), p. 412, cited in ref. 54.
57. K. Torronen, T. Saario, H. Hanninen, M. Kemppainen, and S. Salonen, The effect of inclusions on the environmentally accelerated cyclic crack growth of reactor pressure vessels in simulated LWR environments, *Proceedings of the 4th ECF Conference*, Vol. II (K. L. Maurer and F. E. Matzer, eds.), EMAS Ltd, Warley, (1982), p. 539.

Accepted January 1992.